NMR studies of changes in subcellular water compartmentation in parenchyma apple tissue during drying and freezing

Brian P. Hills* & Benoit Remigereau

Institute of Food Research, Norwich Research Park, Colney, Norwich NR4 7UA

Summary The potential of Nuclear Magnetic Resonance (NMR) and Magnetic Resonance Imaging (MRI) for non-invasively monitoring the subcellular and intercellular redistribution of water in cellular tissue during drying and freezing processes is assessed and it is concluded that despite exciting advances in NMR micro-imaging and NMR microscopy, nonspatially resolved NMR relaxation and diffusion techniques still provide the best probes of subcellular water compartmentation in tissue. The power of the NMR relaxation technique is illustrated by using the changes in the distribution of NMR water proton transverse relaxation times to monitor the subcellular compartmentation of water and ice during the drying and freezing of parenchyma apple tissue. The NMR drying data are analysed with a numerical model of the cell and show that mild air-drying in a fluidized bed results in loss of water from the vacuolar compartment, but not from the cytoplasm or cell wall regions. The loss of vacuolar water is associated with overall shrinkage of the cell and only a slight increase in air space. During freezing the vacuolar compartment is found to be the first to freeze, with the cytoplasmic and cell wall compartments only freezing at much lower temperatures. Freeze-drying apple tissue gives much lower water contents than fluidized bed drying, but the NMR data confirms that it destroys membrane integrity and causes cell wall collapse.

Keywords Cell walls, cell-water modelling, fluid-bed drying, freeze-drying, membrane damage, MRI.

Introduction

Optimization of food quality and cost effectiveness in drying and freezing processes is of crucial importance in the food manufacturing industry and requires a fundamental understanding of water relationships in foods. The macroscopic transport of water through the cellular tissue constituting fruit and vegetables during drying is largely controlled by the microscopic distribution of water and air on a cellular and subcellular distance scale and by the magnitude of membrane permeability barriers. Similarly, the rate of heat transport through the tissue during freezing will depend on factors such as the microscopic distribution of unfrozen water and ice among the subcellular organelles. It is therefore essential to develop non-invasive techniques for investigating the subcellular compartmentation of water and ice during drying and freezing operations.

Optical and electron microscopy are obvious techniques to use but they suffer from artefacts introduced during sample preparation and, without extensive image analysis, provide only qualitative information. For example, it would be very difficult to determine the amount of unfrozen water and its subcellular distribution in a partly frozen tissue with optical or electron microscopy. On the other hand Nuclear Magnetic Resonance (NMR) and Magnetic Resonance Imaging (MRI)

*Correspondent: Fax: +44 1603 507723.
e-mail: Hillsb@bbsrc.ac.uk

techniques are unique in their ability to provide this information. Being non-invasive NMR does not introduce processing artefacts and permits repeated observation on the same sample as it undergoes controlled changes during processing, development or storage. Moreover, the total proton NMR signal from any region of the sample is directly proportional to the proton density, so the technique is quantitative.

A disadvantage of NMR is its low sensitivity, which is the major factor limiting spatial resolution in NMR microscopy, although other factors such as relaxation and diffusion can also limit the resolution (Callaghan, 1991; Hills *et al*., 1990). The potential of NMR micro-imaging in following changes in fruit and vegetable tissue during development, bruising and disease damage has been reviewed (Goodman & Glidewell, 1995) and quantitative relaxation time, spin-density, and diffusion maps for different tissue types have been reported for maize plants (Kuchenbrod *et al*., 1995) and in cultivated strawberry fruit (Goodman *et al*., 1996). Nevertheless NMR micro-imaging is still in its developmental stages and the authors are unaware of any attempts to use the technique to follow tissue structure changes during drying or freezing. Moreover spatial resolutions in NMR micro-imaging (typically of the order of 40 microns or more) are insufficient to resolve subcellular water compartments, though individual cells in the tissue are often distinguishable. The long image acquisition times required for this degree of spatial resolution are also too long to permit real-time, in-probe monitoring of the tissue changes associated with freezing or drying, though slower changes caused by infection or ripening are readily followed.

Higher spatial resolutions of the order of 5–20 microns can be achieved with purpose-built NMR microscopes, allowing visualization of gross intracellular structures in large single plant cells (Aitken *et al*., 1995; Bowtell *et al*., 1995). In principle, NMR microscopy could permit subcellular compartmentation to be directly imaged as cellular tissue undergoes processing, but this has yet to be achieved and few laboratories are currently equipped to perform these measurements. Another current limitation of NMR microscopy is the small sample size (typically a millimetre or less) needed to achieve these very high spatial resolutions. This means that real-time imaging of subcellular changes during the processing of large pieces of cellular tissue are still beyond the current capability of the technique.

Somewhat ironically, subcellular water compartmentation can be monitored in large tissue samples using non-spatially resolved NMR techniques. This is possible because water in different subcellular organelles is often characterized by different proton relaxation times. The distribution of water proton transverse relaxation times can therefore provide quantitative information about water compartmentation. In addition the extent to which water diffusion is restricted by membrane and cell wall barriers can also be measured by non-spatially resolved NMR diffusion techniques and these provide valuable information about membrane permeability coefficients. The potential of NMR relaxation and diffusion measurements in monitoring water compartmentation and in determining membrane permeabilities in intact tissue were explored theoretically and experimentally in several earlier papers (Hills & Duce, 1990; Hills & Snaar, 1992; Snaar & Van As, 1992). One major disadvantage of these relaxation and diffusion techniques highlighted by these earlier studies was their dependence on numerical models of inter-compartmental diffusion and relaxation for quantitative data interpretation. This remains a limitation, but, pending developments in NMR micro-imaging and NMR microscopy, the relaxation–diffusion approach remains the most powerful tool currently available for monitoring subcellular water compartmentation.

Most NMR and MRI studies of plant tissue have been concerned with intact tissue or tissue undergoing relatively slow physiological changes due to ripening or infection. There have been relatively few quantitative studies of water transport and distribution in cellular tissue during more rapid physical processes such as drying or freezing. A number of MRI studies have imaged macroscopic moisture gradients during the drying of potato (Ruan *et al*. 1991) and apple (McCarthy *et al*., 1994) and the macroscopic gradients were modelled as a Fickian diffusion process with a water self-diffusion coefficient dependent on local water content. However, the more fundamental relationship between the

macroscopic water diffusivity and the subcellular water redistribution has yet to be explored by NMR, although theoretical models relating tissue microstructure to macroscopic transport processes in cellular foods have been in the literature for many years (see, for example, Rotstein & Cornish, 1978). The first step in using NMR to relate the subcellular to macroscopic transport properties is to develop NMR methods for monitoring the changes in subcellular water compartmention as a function of water content and temperature, but in the absence of macroscopic moisture or temperature gradients. This is the subject of the present paper and builds on our earlier study of potato freezing using NMR relaxation time distributions (Hills & LeFloch, 1994). The second step is to combine the subcellular compartmentation methods with the macroscopic imaging methods to develop a microscopic understanding of the macroscopic drying or freezing process. This remains a challenge for future work.

In this paper we therefore focus on the first of these two stages and use NMR water proton relaxation time distributions to monitor changes in subcellular water compartmentation in the parenchyma tissue of apple during drying, freezing and rehydration.

As we shall explain in the results section, artifacts arising from the difference in magnetic susceptibility between water and air dominate our non-spatially resolved water diffusion measurements on the apple tissue so, in this study, we have not been able to exploit the additional information available from NMR diffusion measurements. Nevertheless this is not a general limitation on NMR diffusion studies and recent developments in NMR q-space microscopy (Callaghan, 1991) and super-con fringe-field NMR diffusion measurements (Kimmich *et al.*, 1994) make diffusion studies of water compartmentation increasingly attractive.

Experimental

NMR measurements

All NMR relaxation measurements were carried out on a Bruker MSL100 spectrometer operating at 100 MHz, using a thermostated, high-power probe with a 90° pulse length of *c.* 2 μs. Tranverse relaxation time distributions were measured using the Carr-Purcell-Meiboom-Gill (CPMG) pulse sequence and the 90–180° pulse spacing was varied between 200 μs and 6 ms. Data were averaged over eight acquisitions and a recycle delay of 10 s was used to avoid saturation. The echo decay envelopes were analysed as a continuous distribution of exponential relaxation times with the CONTIN program (Provencher, 1982).

Sample processing

Drying in a fluidized bed was performed using 1-cm^3 cubes of parenchyma tissue cut from golden delicious apples. Drying was performed at 295 K with the air blower set at 18 L s^{-1}. The cubic samples were weighed before and immediately after drying for specified times and their volumes were estimated by measuring their three linear dimensions. For NMR measurements the partly dried cubes were wrapped in cling-film to prevent further moisture loss and stored for 24 h at 274 K before measurements were commenced in order to permit equilibration of any moisture gradients set up in the cube during air-drying. The effect of biological variation was investigated by deliberately comparing the amplitudes and durations of the transverse relaxation components for parenchyma tissue from unripe, ripe and overripe golden delicious apples. The difference in the relaxation parameters between samples was no greater than 15%. Nevertheless, to minimize variation in all subsequent experiments parenchyma tissue was taken from the same batch of ripe apples.

The freeze-dried apple was purchased commercially and rehydrated to varying degrees by addition of the calculated weight of distilled water at 295 K. The freeze-thawing experiments were performed in the NMR probe in the standard way by evaporating liquid nitrogen and passing the cold gas through the probe.

Drying results

The subcellular distribution of water in fresh apple tissue

Figure 1 shows the distribution of water proton transverse relaxation times measured at 100 MHz

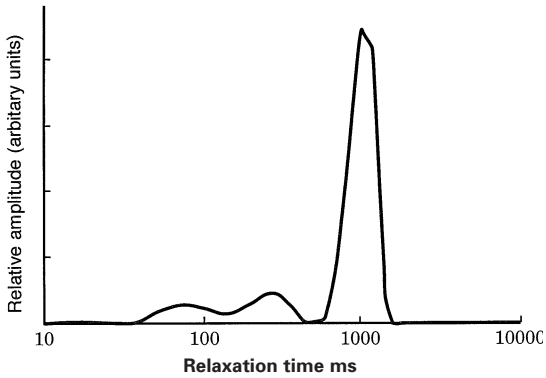

Figure 1 The distribution of transverse water proton relaxation times in fresh, undried parenchyma tissue measured at a spectrometer frequency of 100 MHz and a CPMG 90–180° pulse spacing of 200 μs at 298 K.

using the CPMG pulse sequence with a 90–180° pulse spacing of 200 μs. Very roughly, the three relaxation time peaks located between 800 and 1000, 200 and 400, and 20 and 80 ms can be assigned to water located in the vacuolar, cytoplasm and cell wall compartments, respectively (Hills & Duce, 1990; Duce *et al.*, 1992). The relative amplitudes of these relaxation peaks are 85, 10 and 5%, showing that the vast majority of the water resides in the vacuolar compartment. The fact that three distinct peaks are seen in Fig. 1 shows that exchange of water by molecular diffusion between the three cell compartments is slow on the NMR relaxation timescale and implies that the tonoplast and plasmalemma membranes are significant permeability barriers to water exchange. The values of the membrane permeabilities and of the intrinsic relaxation times of water in the subcellular compartments of the fresh parenchyma tissue can be estimated by fitting the relaxation data in Fig. 1 with the numerical cell model which is discussed in the next section. This was reported in a previous publication where the relaxation data was combined with stimulated echo studies of water diffusivity in the apple tissue (Hills & Snaar, 1992).

It is known that *c.* 20–25% of the total volume of apple consists of intercellular air space. Because of the difference in magnetic susceptibility between water and air, these intercellular air spaces give rise to significant inhomogeneous magnetic field gradients when the tissue is placed in the main magnetic field of an NMR spectrometer. The diffusion of water through these localized field gradients causes rapid dephasing of the transverse magnetization which is manifested as a shortening of the transverse relaxation times as the CPMG 90–180° pulse spacing is increased. This effect is seen experimentally in Fig. 2 and has been discussed in detail in a previous publication (Hills & Duce, 1990). Because of the complexities introduced by the enhanced dephasing at long CPMG pulse spacings, most of the experiments reported in this paper were undertaken with a short CPMG pulse spacing of 200 μs, unless otherwise stated.

Partially dried parenchyma apple tissue

Figure 3 shows the experimental drying curve for 1-cm^3 cube samples of apple tissue and shows that under the conditions pertaining in the fluidized bed drier the weight loss could not exceed *c.* 60%. Figure 4 shows the mass loss is accompanied by a corresponding decrease in volume of the apple cubes. The slight departure from linearity seen in Fig. 4 corresponds to a slight density decrease during drying corresponding, presumably, to a slight increase in the volume of intercellular air gaps. Examination of the apple samples after drying revealed that the turgor pressure was still significant because the tissue still appeared and felt 'fresh', suggesting that membrane integrity had been maintained and the cell walls had not collapsed.

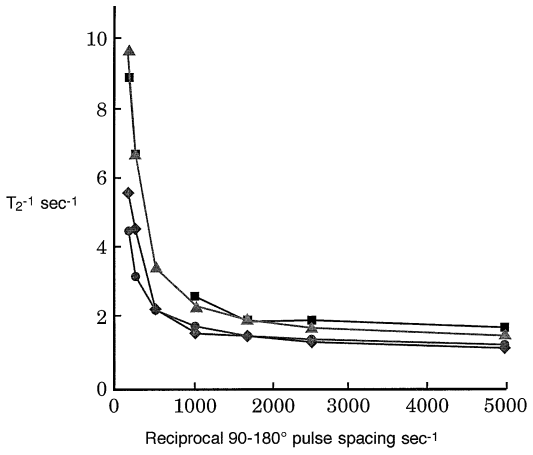

Figure 2 Dependence of the vacuolar-water transverse relaxation rate on reciprocal 90–180° CPMG pulse spacing (s^{-1}) for parenchyma apple tissue dried to the indicated extents. ◆ 0, ● 32, ▲ 48, ■ 64%, water loss.

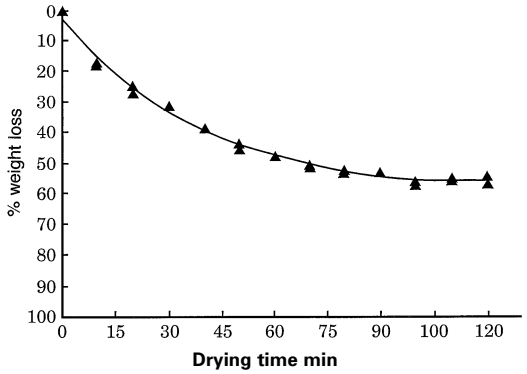

Figure 3 The experimental drying curve for 1-cm³ cubes of apple tissue dried in a fluidized bed under the conditions described in the text. The line is the least squares fit to the data.

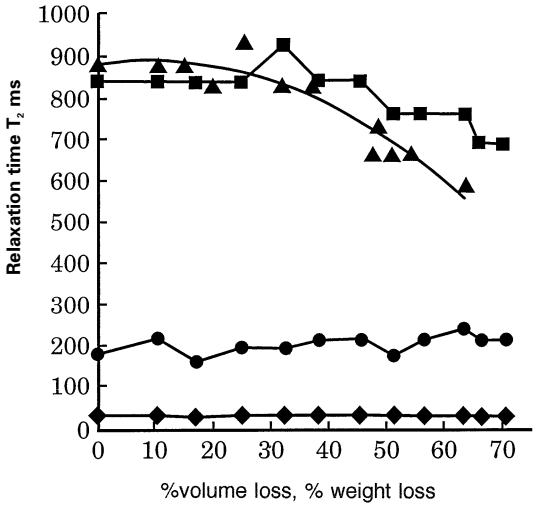

Figure 5 Simulation of the dependence of the transverse relaxation time peak positions on water content using the numerical cell model. (▲) experiment (line is guide to the eye); calculated position of the (■) vacuole (●) cytoplasm (◆) cell wall.

While useful, these 'macroscopic' observations of drying do not reveal the microscopic redistribution of water between the subcellular compartments as the drying proceeds. This information can be obtained from the changes in the water proton relaxation time distributions. The shifts in position of the three relaxation time peak maxima seen in Fig. 1 are plotted in Fig. 5 as a function of the percentage water loss. The major change is seen to be a reduction in the relaxation time of the water in the vacuolar compartment from *c*. 900 ms to 600 ms as the tissue water is reduced to 60%. At the same time the cytoplasmic and cell wall relaxation times remain roughly constant at 180 ms and 40 ms, respectively. Figure 6 shows that the reduction in the vacuolar relaxation time is accompanied by a reduction in its relative area from *c*. 85 to 35%.

Knowing these subcellular changes and the overall mass and density changes it is possible to draw some important conclusions about the drying process. Figure 4 shows that when the average tissue mass decreases by 57% there is an

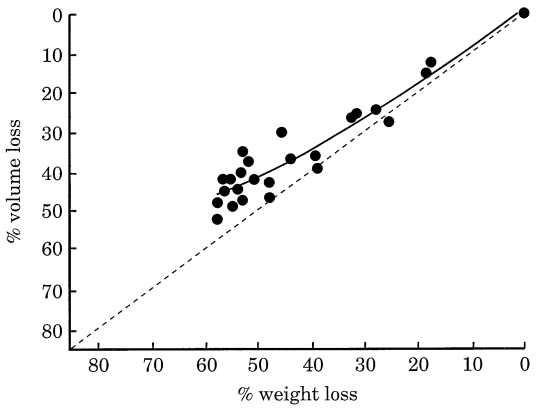

Figure 4 Comparison of the experimental % volume loss vs. % weight loss during drying of apple tissue. Note the slight reduction in density at lower water contents.

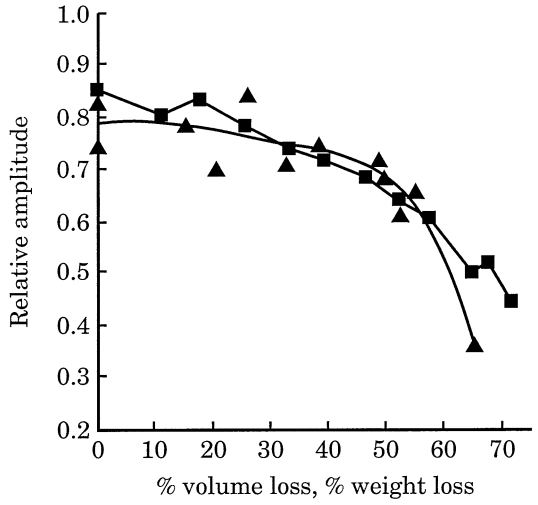

Figure 6 Simulation of the dependence of the relative area of the vacuolar transverse relaxation time peak on water content using the numerical cell model. (▲) experiment (line is guide to the eye); simulation (■).

average volume reduction of 45% and an 11% increase in the average air space volume. At the same time the relative amplitude of the vacuolar relaxation peak decreases by *c*. 45%. This shows that the water is lost primarily from the vacuolar compartment and not from the cytoplasm or cell wall and that the loss of water from the vacuole is accompanied by an overall volume shrinkage of the whole cell. If this is the case then it should be possible to numerically model the observed changes in the relaxation time distributions simply by reducing the cell and vacuolar volumes while keeping the cytoplasmic and cell wall volumes constant. These calculations are presented in the next section. If this interpretation is correct, then the slight increase in the intercellular air spaces in the dried tissue should also result in enhanced dephasing contributions at long CPMG pulse spacings. These data are presented in Fig. 2 where the general increase is observed, but because the local induced field gradients depend on the size, geometry and distribution of the air gaps, the enhanced dephasing is not a regular function of the water loss as might have been expected.

Interpretation of the NMR drying data with the numerical cell model

The numerical cell model has been described in detail in a previous publication (Hills & Snaar, 1992). It approximates the parenchyma tissue as a collection of identical spherical cells, each comprising three concentric spherical compartments corresponding to the vacuole, cytoplasm and cell wall. These are separated by the tonoplast and plasmalemma membranes of thickness w(1) and w(2), respectively (see Fig. 7). As indicated in Fig. 7, each subcellular compartment, *n*, is characterized by an intrinsic water self diffusion coefficient, D_n, and water proton transverse relaxation time, $T_2(n)$. The membranes are characterized by a width, w(m), water self diffusion coefficients, $D_{mem}(m)$, and intrinsic relaxation times, $T_{mem}(m)$, where m is 1 for the tonoplast and 2 for the plasmalemma. This corresponds to membrane permeability coefficients, P(m) of $D_{mem}(m)/w(m)$. The relaxation and diffusion of the water proton transverse magnetization is calculated by solving the Bloch-Torrey equations (Torrey, 1956) within all five compartments. This is done by numerical integration using a standard finite difference algorithm within a spherical coordinate system. Because the tonoplast, cytoplasm, plasmalemma and cell wall regions are relatively thin regions on the outside of the sphere it is necessary to improve the accuracy of the calculation in the outer regions by placing more mesh points at larger radii, according to the relation:

$$r_i = r_{max} \sin[0.5\pi\ (i - 1)/(i_{max} - 1)] \qquad (1)$$

where r_i is the location of the meshpoint i and r_{max}

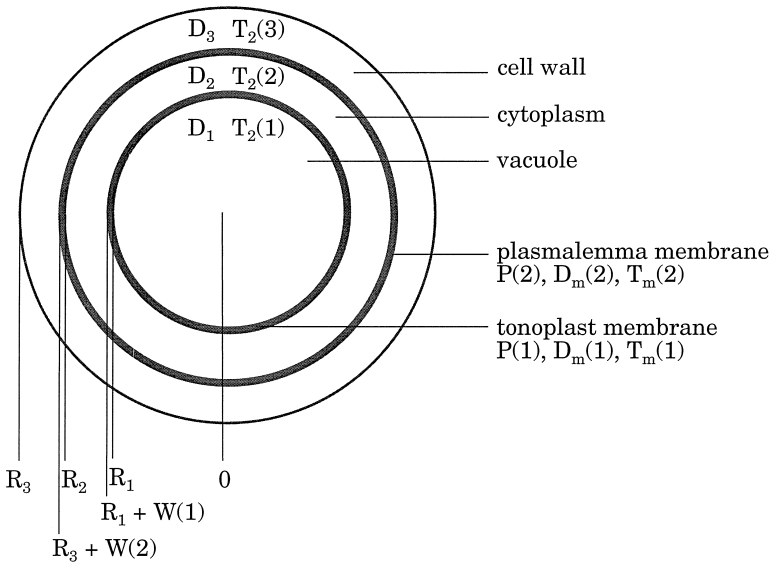

Figure 7 The numerical, spherical-cell model. The Bloch-Torrey equations are solved in each of the three aqueous compartments and two membrane regions with the parameters indicated in the diagram and in Table 1. The labels D, T and P refer to the intrinsic water self-diffusion coefficients, water proton transverse relaxation times and membrane permeabilities, respectively.

is the total number of mesh points, typically about 200.

Estimates of the parameters corresponding to the fresh, undried tissue have been made in a previous work by fitting experimental NMR relaxation and diffusion data (Hills & Snaar, 1992). To simulate the effect of drying we assume, according to the above discussion, that drying removes water only from the vacuolar compartment, resulting in a size reduction of the whole cell, while leaving the volumes of the cytoplasm and cell wall compartments constant. This requires careful calculation of the positions of the new 'shrunken' mesh points using equation [1] and assumes that all other parameters, including membrane permeabilities, diffusion coefficients and intrinsic relaxation times are unaffected by the cell shrinkage. In principle, the concentration of the vacuolar fluid may result in a decrease in its intrinsic relaxation time, but this effect has been ignored.

Figures 5 and 6 include a comparison of the theoretical drying results for the parameter set listed in Table 1 with the experimental data for the relaxation time peak maxima and their relative amplitudes. It can be seen that the general trend is reasonably well reproduced, especially the fall in relaxation time and relative amplitude of the vacuolar contribution as a function of water loss. Perfect agreement is, however, not to be expected because the cells are rarely totally spherical and there is a cell size distribution within the tissue. Nevertheless the model does show that the main changes in the NMR data can be understood as a simple loss of water from the vacuole resulting in an overall shrinkage of the cell.

Table 1 Parameter values in the numerical cell model (see Fig. 7)

Parameter	Symbol	Value
Initial cell radius (μm)	R_3	50
Cytoplasmic size (μm)	R_2	48.59
Vacuole size (μm)	R_1	45.48
Tonoplast width (μm)	w(1)	0.636
Plasmalemma width (μm)	w(2)	0.349
Vacuole relaxation rate (s^{-1})	$T_2(1)^{-1}$	1.05
Cytoplasm relaxation rate (s^{-1})	$T_2(2)^{-1}$	2.7
Cell wall relaxation rate (s^{-1})	$T_2(3)^{-1}$	25
Tonoplast relaxation rate (s^{-1})	$T_m(1)^{-1}$	0.01
Plasmalemma relaxation rate (s^{-1})	$T_m(2)^{-1}$	0.01
Vacuole diffusion coeff (cm^2s^{-1})	D_1	$2.2.10^{-5}$
Cytoplasm diffusion coeff (cm^2s^{-1})	D_2	$1.5.10^{-6}$
Cell wall diffusion coeff (cm^2s^{-1})	D_3	$1.5.10^{-7}$
Tonoplast diffusion coeff (cm^2s^{-1})	$D_m(1)$	$5.0.10^{-8}$
Plasmalemma diffusion coeff (cm^2s^{-1})	$D_m(2)$	$1.0.10^{-8}$

Rehydration of freeze-dried apple tissue

It is interesting to compare the previous NMR relaxation distributions for mild drying in a

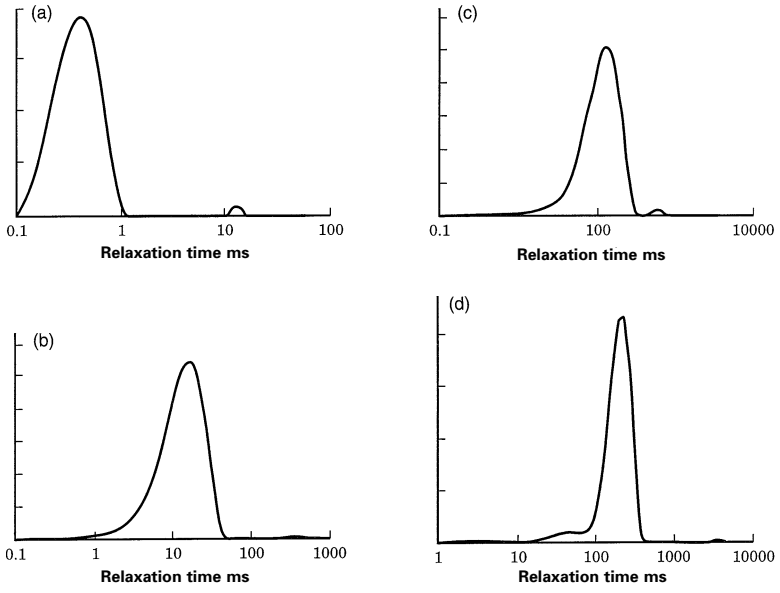

Figure 8 Experimental transverse relaxation time distributions for freeze-dried apple rehydrated to the indicated water contents and measured at a spectrometer frequency of 100 MHz at a CPMG pulse spacing of 200 μs at 298 K.

fluidized bed with the more dramatic drying obtained with freeze-drying which gives a much lower final water content and usually results in membrane damage, cell wall collapse and loss of turgor. Figure 8, curve (a) shows the transverse relaxation time distributions for apple tissue freeze-dried to *c*. 28% by weight water. The large relaxation time peak between 0.1 and 1 ms most probably corresponds to the 'solid-like' signal from protein, polysaccharide, lipid and residual 'bound' water protons. The much smaller peak at *c*. 10 ms is interesting because it progressively increases in relative amplitude as the tissue is rehydrated to *c*. 46%, indicating that the additional water forms a protein and metabolite solution. As the tissue is further rehydrated this peak shifts to longer relaxation times and remains essentially unimodal. A small peak between 10 and 70 ms does appear in the fully rehydrated, freeze-dried tissue (see Fig. 8d) but this probably results from heterogeneity in the tissue and water-filled air-gaps. These results confirm the very important effect of the low membrane permeabilities in maintaining compartmentation in the tissue. When the membranes are intact the relaxation is trimodal and the dominant vacuolar peak appears in the range 600–900 ms, depending on the water content. In contrast, loss of membrane integrity resulting from freeze-drying results in single exponential relaxation and much shorter relaxation times. This contrast is shown in Fig. 9 and illustrates the sensitivity of NMR relaxation in monitoring subcellular water compartmentation.

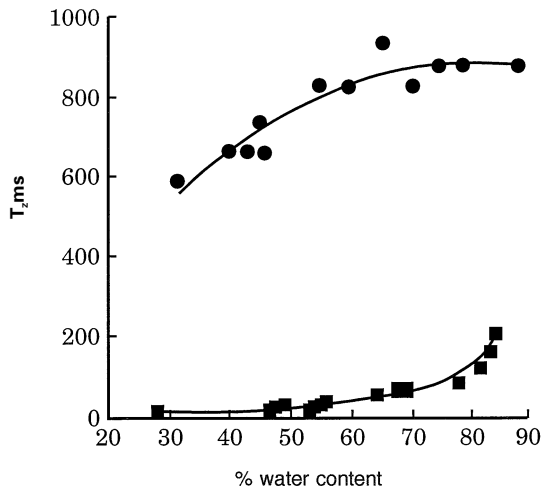

Figure 9 A comparison of the water proton transverse relaxation times (milliseconds) for water in frozen-thawed apple tissue (●) and in rehydrated freeze-dried apple tissue (■).

Freeze-thawing studies

Water compartmentation in cellular tissue can also be affected by freezing and thawing since not all water compartments freeze and thaw at the same temperature. This is an extremely important phenomenon because the formation and distribution of ice crystals in cellular tissue during freezing largely determines whether the cell and organelles retain turgor pressure and impart a fresh texture on thawing. NMR relaxometry is a useful tool in these studies since it permits the non-invasive examination of the freezing-thawing behaviour of subcellular compartments. This is

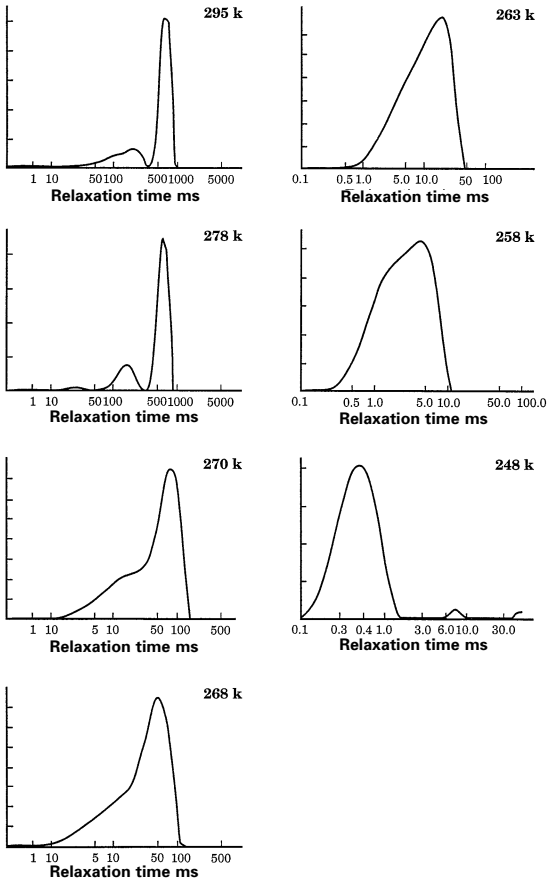

Figure 10 Transverse relaxation time distributions during the freezing of apple tissue from 295 K to 248 K.

possible because ice has a proton tranverse relaxation time of only a few microseconds so it is invisible on the millisecond timescale used in the NMR CPMG measurements. The freezing of a subcellular compartment therefore results in the disappearance of its associated peak in the relaxation time distribution.

Figure 10 shows the changing water proton transverse relaxation time distributions as parenchyma apple tissue is progressively frozen inside the NMR probe. At each temperature the sample was allowed to equilibrate for at least 15 min. Between 295 and 278 K no changes appear except a slight decrease in the vacuolar relaxation time from 652 to 521 ms. At 270 K the vacuolar peak has vanished showing that the vacuolar compartment has frozen. However, the two peaks corresponding to the cytoplasm and cell wall compartments located between 1 and 100 ms remain essentially unchanged at this temperature, indicating that these compartments remain unfrozen. The temperature has to be lowered to *c*. 263 K before the cytoplasm freezes and even at this temperature there is still a relaxation peak between 1 and 50 ms, most probably arising from unfrozen water in the cell wall compartment. By 248 K even this peak is removed and a new peak appears between 0.1 and 1 ms, most probably corresponding to unfrozen water associated with macromolecules because similar peaks are observed when protein solutions are frozen (Kuntz & Kauzman, 1974).

The relaxation time distributions as the frozen tissue is thawed from 248 K to room temperature are very similar to the freezing results showing the absence of any hysteresis in the freeze-thawing cycle, at least up to the point when the vacuole melts. However, it is noteworthy that the relaxation time of the frozen-thawed vacuole at room temperature is only 250 ms compared to the value of *c*. 650 ms in the fresh tissue (see Fig. 11). Moreover, the cell wall and cytoplasm compartments are not so clearly resolved in the room temperature freeze-thawed sample. Indeed the room-temperature freeze-thawed distribution more closely resembles that of the rehydrated freeze-dried sample than that of the fresh tissue (see Fig. 11) which is consistent with membrane rupture and loss of turgor in the tissue.

The ability of NMR to resolve the freezing of different subcellular compartments has not yet been fully exploited in plant science. It would be especially interesting to compare the results for different rates of freezing which are known to control the size distribution of the ice crystals and can give rise to severe undercooling. The effect of cryoprotectants such as trehalose on compartmental freezing would also be an interesting topic for investigation.

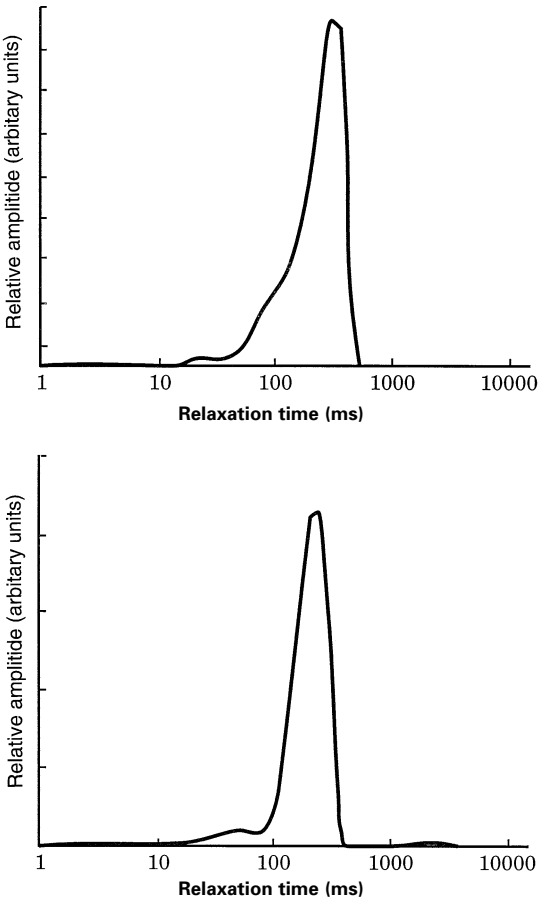

Figure 11 A comparison of the transverse relaxation time distribution for freeze-thawed apple tissue and fully rehydrated freeze-dried apple (water content = 86% w/w).

Discussion and conclusion

Our results illustrate the power of NMR relaxometry for monitoring subcellular water compartmentation. Air-drying parenchyma apple tissue is shown to result in loss of water from the vacuolar compartment with very little change in the water content of either the cytoplasm or the

cell wall compartments. Apparently the apple cell wall framework is sufficiently flexible that loss of water from the vacuole results in shrinkage of the whole tissue rather than simply an increase in the volume of intercellular air-gaps with little or no shrinkage. The freezing results show that the vacuolar compartment is the first to freeze at *c.* 270 K but, because of their higher biopolymer content, the cytoplasm and cell wall compartments require temperatures below 263 K before they freeze. These changes largely parallel those previously found for potato except that freeze-thawing hysteresis is not observed with apple under the conditions used here. The extent to which this behaviour applies to different plant cells in non-parenchyma tissue remains to be investigated. Prelimary results on carrot tissue show that, in this sample, high solute concentrations dominate the NMR relaxation time distributions and cause very different drying and freezing behaviour at the subcellular level. We hope to report these results in the near future.

No NMR water diffusion measurements on the apple tissue have been reported in this paper. This is because diffusion measurements can only be made at a higher spectrometer frequency of 300 MHz on a Bruker MSL300 spectrometer in our laboratory, and at this high field strength the internally induced, inhomogeneous magnetic field gradients around the air-gaps in apple tissue cause extraordinary enhancements in the apparent water diffusivity by several orders of magnitude. The quantitative interpretation of these enhancements is itself of interest and is reported elsewhere (Hills *et al.*, 1996), but they are of little value in providing diffusion coefficients for input into the numerical cell model. Accordingly only the classic low-field pulsed gradient, stimulated-echo diffusion measurements on apple first reported by Tanner & Stejskal (1968) were used to estimate the tonoplast membrane permeability in our previous publication (Hills & Snaar, 1992).

The feasibility of combining our relaxation time distributions with volume selective excitation in micro-imaging during drying and freezing remains an attractive, but unexplored, possibility. This would be especially valuable for tissue samples having a less homogeneous cell distribution than parenchyma tissue in apple. To do this it will be necessary to acquire considerably larger data sets than those currently used in conventional relaxation-weighted imaging studies. For example a conventional relaxation time map in imaging is usually derived with the assumption that the relaxation is single exponential so only sufficient delay times for a single exponential fit are acquired. In contrast, the multiple exponential CPMG echo decay envelopes used to calculate the relaxation time distributions reported in this paper typically require 1–16 K echoes. We have recently shown, using a model sample, that it is possible to observe multiple-exponential relaxation in micro-imaging by increasing the number of echo decays in the imaging sequence (Hills & Babonneau, 1994), but this was only achieved at the expense of greatly increased acquisition time. Multiple exponential transverse relaxation in images of degenerating peripheral nerve has also been reported recently (Does & Snyder, 1996). Achieving multiple exponential imaging in a real-time processing situation will require the development of much faster imaging protocols and remains a challenge for the future.

Acknowledgements

The authors gratefully acknowledge the financial support of the BBSRC and wish to thank Professor M.L. Martin of the University of Nantes for permitting B. Remigereau to undertake this work as part of a D.E.A. mention Europeenne under the ERASMUS scheme.

References

Aitken, N.R., Hsu, E.W. & Blackband, S.J. (1995). A review of NMR microimaging studies of single cells. *Journal of Magnetic Resonance Analysis*, **1**, 41–48.

Bowtell, R.W., Peters, A., Sharp, J.C., Mansfield, P., Hsu, E.W., Aiken, N., Horsman, A. & Blackburn, S.J. (1995). NMR microscopy of single neurons using spin-echo and line narrowed 2D-FT imaging. *Magnetic Resonance in Medicine*, **33**, 790–794.

Callaghan, P.T. (1991). *Principles of Nuclear Magnetic Resonance Microscopy*. Pp. 173–226. Oxford: Oxford Science Publications.

Does, M.D. & Snyder, R.E. (1996). Multiexponential T_2 relaxation in degenerating peripheral nerve. *Magnetic Resonanace in Medicine*, **35**, 207–213.

Duce, S.L. Carpenter, T.A., Hall, L.D. & Hills, B.P. (1992). An investigation of the origins of contrast in spin-echo images of plant tissue. *Magnetic Resonance Imaging*, **10**, 289–297.

Goodman, B.A. & Glidewell, S.M. (1995). High field NMR microscopy of agricultural produce. *Microscopy and Analysis,* November 1995.

Goodman, B.A., Williamson, B., Simpson, E.J., Chudek, J.A., Hunter, G. & Prior, D.A.M. (1996). High field NMR microscopic imaging of cultivated strawberry fruit. *Magnetic Resonance Imaging*, **14**, 187–196.

Hills, B.P. & Babonneau, F. (1994). Quantitative radial imaging of porous particle beds with varying water contents. *Magnetic Resonance Imaging*, **12**, 1065–1074.

Hills, B.P. & Duce, S.L. (1990). The influence of chemical and diffusive exchange on water proton transverse relaxation in plant tissue. *Magnetic Resonance Imaging* **8**, 321–331.

Hills, B.P. & LeFloch, G. (1994). NMR studies of non-freezing water in cellular plant tissue. *Food Chemistry,* **51**, 331–336.

Hills, B.P. & Snaar, J.E.M. (1992). Dynamic q-space microscopy of cellular tissue, *Molecular Physics*, **76**, 979–994.

Hills, B.P., Wright, K.M. & Belton, P.S. (1990). The effects of restricted diffusion in NMR microscopy. *Magnetic Resonance Imaging,* **8**, 755–765.

Hills, B.P., Wright, K.M. & Snaar, J.E.M. (1996). Dynamic NMR Q-space studies of microstructure with the multigrade CPMG sequence. *Magnetic Resonance Imaging*, **14**, 305–318.

Kimmich, R., Stapf, S., Callaghan, P. & Coy, A. (1994). *Magnetic Resonance Imaging*, **12**, 339.

Kuchenbrod, E., Haase, A., Benkert, R., Scheider, H. & Zimmerman, U. (1995). Quantitative NMR microscopy on intact plants. *Magnetic Resonance Imaging,* **13**, 447–455.

Kuntz, I.D. & Kauzman, W. (1974). Hydration of proteins and polysaccharides, *Advances in Protein Chemistry*, **28**, 239.

McCarthy, M.J., Lasseaux, D. & Maneval, J.E. (1994)., NMR imaging in the study of diffusion of water in foods. *Journal of Food Engineering*, **22**, 211–224.

Provencher, S.W. (1982). A constrained regularization method for inverting data represented by linear algebraic or integral equations. *Computational Physics Communications*, **27**, 213.

Rotstein, E. & Cornish, A.R.H. (1978). Influence of cellular membrane permeability on drying behaviour. *Journal of Food Science*, **43**, 926–934.

Ruan, R., Schmidt, S.J., Schmidt, A.R. & Litchfield, J.B. (1991). Non-destructive measurement of transient moisture profiles and the moisture diffusion coefficient in a potato during drying and adsorption by NMR Imaging. *Journal of Food Process Engineering*, **14**, 297–313.

Snaar, J.E.M. & Van As, H. (1992). Probing water compartments and membrane permeability in plant cells by ^{1}H NMR relaxation measurements. *Biophysics Journal*, **63**, 1654–8.

Tanner, J.E. & Stejskal, E.O. (1968). Restricted self-diffusion of protons in colloidal systems by the pulsed field gradient spin-echo method. *Journal of Chemical Physics*, **49**, 1768.

Torrey, H.C. (1956). Bloch equations with diffusion terms. *Physical Reviews*, **104**, 563.

Received 4 October 1996, revised and accepted 8 February 1997